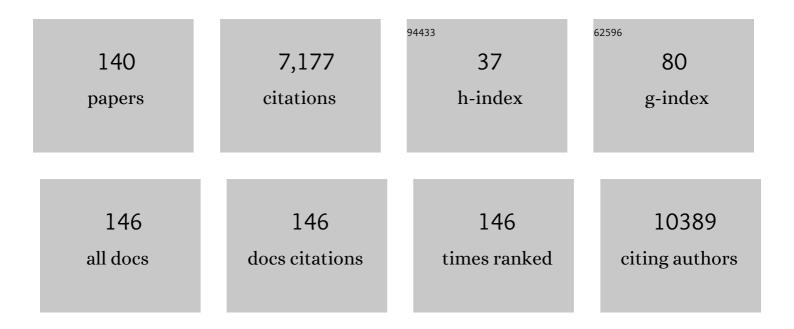
Aleksander Gurlo

List of Publications by Year in descending order

Source: https://exaly.com/author-pdf/979899/publications.pdf Version: 2024-02-01



#	Article	IF	CITATIONS
1	Review of the anatase to rutile phase transformation. Journal of Materials Science, 2011, 46, 855-874.	3.7	2,530
2	Freeze Casting: From Lowâ€Dimensional Building Blocks to Aligned Porous Structures—A Review of Novel Materials, Methods, and Applications. Advanced Materials, 2020, 32, e1907176.	21.0	404
3	Nanosensors: towards morphological control of gas sensing activity. SnO ₂ , In ₂ O ₃ , ZnO and WO ₃ case studies. Nanoscale, 2011, 3, 154-165.	5.6	399
4	Machine Learning for Materials Scientists: An Introductory Guide toward Best Practices. Chemistry of Materials, 2020, 32, 4954-4965.	6.7	224
5	Visible Light Photocatalysis with c-WO _{3–<i>x</i>} /WO ₃ ×H ₂ O Nanoheterostructures In Situ Formed in Mesoporous Polycarbosilane-Siloxane Polymer. Journal of the American Chemical Society, 2013, 135, 4467-4475.	13.7	150
6	Materials and Applications for Low-Cost Ceramic Membranes. Membranes, 2019, 9, 105.	3.0	106
7	Additive manufacturing of ceramics from preceramic polymers: A versatile stereolithographic approach assisted by thiol-ene click chemistry. Additive Manufacturing, 2019, 27, 80-90.	3.0	98
8	Azo dye adsorption on an industrial waste-transformed hydroxyapatite adsorbent: Kinetics, isotherms, mechanism and regeneration studies. Journal of Environmental Chemical Engineering, 2020, 8, 103807.	6.7	93
9	Nanoporous Silicon Oxycarbonitride Ceramics Derived from Polysilazanes In situ Modified with Nickel Nanoparticles. Chemistry of Materials, 2011, 23, 4112-4123.	6.7	78
10	Ab initio study of phase stability in doped TiO2. Computational Mechanics, 2012, 50, 185-194.	4.0	78
11	Metastability of Corundumâ€Type In ₂ O ₃ . Chemistry - A European Journal, 2008, 14, 3306-3310.	3.3	77
12	Synthesis and sensoric response of ZnO decorated carbon nanotubes. Journal of Materials Chemistry, 2009, 19, 5039.	6.7	76
13	Investigation of the role of the Na2WO4/Mn/SiO2 catalyst composition in the oxidative coupling of methane by chemical looping experiments. Journal of Catalysis, 2018, 360, 102-117.	6.2	76
14	Eco-fabrication of hierarchical porous silica monoliths by ice-templating of rice husk ash. Green Chemistry, 2017, 19, 188-195.	9.0	66
15	Polymer-Derived SiOC Integrated with a Graphene Aerogel As a Highly Stable Li-Ion Battery Anode. ACS Applied Materials & Interfaces, 2020, 12, 46045-46056.	8.0	66
16	Thermal decomposition of carbon-rich polymer-derived silicon carbonitrides leading to ceramics with high specific surface area and tunable micro- and mesoporosity. Journal of the European Ceramic Society, 2012, 32, 477-484.	5.7	64
17	Template-free synthesis of polymer-derived mesoporous SiOC/TiO2 and SiOC/N-doped TiO2 ceramic composites for application in the removal of organic dyes from contaminated water. Applied Catalysis B: Environmental, 2012, 115-116, 303-313.	20.2	63
18	Can we predict the formability of perovskite oxynitrides from tolerance and octahedral factors?. Journal of Materials Chemistry A, 2013, 1, 12239.	10.3	61

#	Article	IF	CITATIONS
19	Surface Carbon as a Reactive Intermediate in Dry Reforming of Methane to Syngas on a 5% Ni/MnO Catalyst. ACS Catalysis, 2018, 8, 8739-8750.	11.2	60
20	Monitoring Gas Sensors at Work: Operando Raman–FTIR Study of Ethanol Detection by Indium Oxide. Angewandte Chemie - International Edition, 2013, 52, 3607-3610.	13.8	55
21	In Situ-Determined Catalytically Active State of LaNiO ₃ in Methane Dry Reforming. ACS Catalysis, 2020, 10, 1102-1112.	11.2	55
22	Hydrothermal synthesis of nanocrystalline hydroxyapatite from phosphogypsum waste. Journal of Environmental Chemical Engineering, 2018, 6, 1347-1352.	6.7	54
23	Nanosensors: Does Crystal Shape Matter?. Small, 2010, 6, 2077-2079.	10.0	52
24	Macroporous polymer-derived SiO2/SiOC monoliths freeze-cast from polysiloxane and amorphous silica derived from rice husk. Journal of the European Ceramic Society, 2017, 37, 4809-4820.	5.7	51
25	Theoretical study on copper's energetics and magnetism in TiO2 polymorphs. Journal of Applied Physics, 2013, 113, .	2.5	48
26	New Dion–Jacobson Phase Three-Layer Perovskite CsBa ₂ Ta ₃ O ₁₀ and Its Conversion to Nitrided Ba ₂ Ta ₃ O ₁₀ Nanosheets via a Nitridation–Protonation–Intercalation–Exfoliation Route for Water Splitting. Crystal Growth and Design, 2016, 16, 2302-2308.	3.0	47
27	Coaxial nanofibers of nickel/gadolinium oxide/nickel oxide as highly effective electrocatalysts for hydrogen evolution reaction. Journal of Colloid and Interface Science, 2021, 587, 457-466.	9.4	47
28	Nanocubes or Nanorhombohedra? Unusual Crystal Shapes of Corundum-Type Indium Oxide. Journal of Physical Chemistry C, 2008, 112, 9209-9213.	3.1	46
29	Molecular based, chimie douce approach to 0D and 1D indium oxide nanostructures. Evaluation of their sensing properties towards CO and H2. Journal of Materials Chemistry, 2010, 20, 8311.	6.7	46
30	The Thermal Conductivity of Polymerâ€Derived Amorphous Si–O–C Compounds and Nanoâ€Composites. Journal of the American Ceramic Society, 2016, 99, 281-285.	3.8	44
31	Elucidating the impact of A-site cation change on photocatalytic H ₂ and O ₂ evolution activities of perovskite-type LnTaON ₂ (Ln = La and Pr). Physical Chemistry Chemical Physics, 2017, 19, 22210-22220.	2.8	44
32	Zirconiumâ€Assisted Activation of Palladium To Boost Syngas Production by Methane Dry Reforming. Angewandte Chemie - International Edition, 2018, 57, 14613-14618.	13.8	44
33	Silicate dielectric ceramics for millimetre wave applications. Journal of the European Ceramic Society, 2021, 41, 3879-3894.	5.7	43
34	Orthorhombic In ₂ O ₃ : A Metastable Polymorph of Indium Sesquioxide. Angewandte Chemie - International Edition, 2013, 52, 6531-6535.	13.8	42
35	NH ₃ -assisted synthesis of microporous silicon oxycarbonitride ceramics from preceramic polymers: a combined N ₂ and CO ₂ adsorption and small angle X-ray scattering study. Journal of Materials Chemistry A, 2015, 3, 805-818.	10.3	41
36	Nanoscaled tin dioxide films processed from organotin-based hybrid materials: an organometallic route toward metal oxide gas sensors. Nanoscale, 2012, 4, 6806.	5.6	40

#	Article	IF	CITATIONS
37	On-chip assembly of 3D graphene-based aerogels for chemiresistive gas sensing. Chemical Communications, 2020, 56, 450-453.	4.1	39
38	Steering the Methane Dry Reforming Reactivity of Ni/La ₂ O ₃ Catalysts by Controlled In Situ Decomposition of Doped La ₂ NiO ₄ Precursor Structures. ACS Catalysis, 2021, 11, 43-59.	11.2	38
39	A molecular approach to Cu doped ZnO nanorods with tunable dopant content. Dalton Transactions, 2011, 40, 4307.	3.3	37
40	Structural investigations of La _{0.6} Sr _{0.4} FeO _{3â~Î} under reducing conditions: kinetic and thermodynamic limitations for phase transformations and iron exsolution phenomena. RSC Advances, 2018, 8, 3120-3131.	3.6	37
41	Functionalization of MCM-41 with titanium oxynitride deposited via PECVD for enhanced removal of methylene blue. Journal of Molecular Liquids, 2019, 274, 505-515.	4.9	37
42	Revealing the Mechanism of Multiwalled Carbon Nanotube Growth on Supported Nickel Nanoparticles by in Situ Synchrotron X-ray Diffraction, Density Functional Theory, and Molecular Dynamics Simulations. ACS Catalysis, 2019, 9, 6999-7011.	11.2	36
43	Fabrication of nitrogen-doped TiO2 monolith with well-defined macroporous and bicrystalline framework and its photocatalytic performance under visible light. Journal of the European Ceramic Society, 2014, 34, 809-816.	5.7	35
44	Transmission <i>in situ</i> and <i>operando</i> high temperature X-ray powder diffraction in variable gaseous environments. Review of Scientific Instruments, 2018, 89, 033904.	1.3	33
45	Highâ€pressure highâ€temperature synthesis of Rh ₂ O ₃ â€llâ€type In ₂ O ₃ polymorph. Physica Status Solidi - Rapid Research Letters, 2008, 2, 269-271.	2.4	32
46	Multilayer Amorphousâ€6iâ€Bâ€Câ€N/γâ€Al ₂ O ₃ /αâ€Al ₂ O ₃ Membranes for Hydrogen Purification. Advanced Engineering Materials, 2010, 12, 522-528.	3.5	32
47	On the structural stability of crystalline ceria phases in undoped and acceptor-doped ceria materials under <i>in situ</i> reduction conditions. CrystEngComm, 2019, 21, 145-154.	2.6	32
48	Structural Stability of Highâ€Pressure Polymorphs in In ₂ O ₃ Nanocrystals: Evidence of Stressâ€Induced Transition?. Angewandte Chemie - International Edition, 2010, 49, 5610-5612.	13.8	31
49	Surface chemistry of pure tetragonal ZrO ₂ and gas-phase dependence of the tetragonal-to-monoclinic ZrO ₂ transformation. Dalton Transactions, 2017, 46, 4554-4570.	3.3	31
50	Hybrid Organotin and Tin Oxide-based Thin Films Processed from Alkynylorganotins: Synthesis, Characterization, and Gas Sensing Properties ACS Applied Materials & Interfaces, 2014, 6, 17093-17101.	8.0	28
51	Removal of cationic and anionic textile dyes with Moroccan natural phosphate. Journal of Environmental Chemical Engineering, 2017, 5, 2189-2199.	6.7	28
52	Bilayer graded Al/B ₄ C/rice husk ash composite: Wettability behavior, thermo-mechanical, and electrical properties. Journal of Composite Materials, 2018, 52, 3745-3758.	2.4	27
53	Improving the physicochemical properties of Y zeolite for catalytic cracking of heavy oil via sequential steam-alkali-acid treatments. Microporous and Mesoporous Materials, 2020, 294, 109854.	4.4	27
54	In situ formation of tungsten oxycarbide, tungsten carbide and tungsten nitride nanoparticles in micro- and mesoporous polymer-derived ceramics. Journal of Materials Chemistry A, 2014, 2, 10454.	10.3	26

#	Article	IF	CITATIONS
55	High-Temperature Stability and Saturation Magnetization of Superparamagnetic Nickel Nanoparticles in Microporous Polysilazane-Derived Ceramics and their Gas Permeation Properties. ACS Applied Materials & Interfaces, 2014, 6, 12270-12278.	8.0	26
56	Reactive metal-support interaction in the Cu-In ₂ O ₃ system: intermetallic compound formation and its consequences for CO ₂ -selective methanol steam reforming. Science and Technology of Advanced Materials, 2019, 20, 356-366.	6.1	26
57	Highâ€Sensitivity Hydrogen Detection: Hydrogenâ€Induced Swelling of Multiple Cracked Palladium Films on Compliant Substrates. Angewandte Chemie - International Edition, 2011, 50, 10130-10132.	13.8	25
58	Surfactant-free self-assembly route to hollow In2O3 microspheres. Chemical Communications, 2009, , 2747.	4.1	24
59	The contrasting effect of the Ta/Nb ratio in (111)-layered B-site deficient hexagonal perovskite Ba ₅ Nb _{4â^x} Ta _x O ₁₅ crystals on visible-light-induced photocatalytic water oxidation activity of their oxynitride derivatives. Dalton Transactions, 2016, 45, 12559-12568.	3.3	24
60	Clay in situ resource utilization with Mars global simulant slurries for additive manufacturing and traditional shaping of unfired green bodies. Acta Astronautica, 2020, 174, 241-253.	3.2	23
61	Tailoring of ordered mesoporous silica COK-12: Room temperature synthesis of mesocellular foam and multilamellar vesicles. Microporous and Mesoporous Materials, 2018, 267, 142-149.	4.4	22
62	A study on the thermal conversion of scheelite-type ABO ₄ into perovskite-type AB(O,N) ₃ . Dalton Transactions, 2015, 44, 8238-8246.	3.3	21
63	Towards the colonization of Mars by in-situ resource utilization: Slip cast ceramics from Martian soil simulant. PLoS ONE, 2018, 13, e0204025.	2.5	21
64	Low-temperature H2sensing in self-assembled organotin thin films. Chemical Communications, 2011, 47, 1464-1466.	4.1	20
65	Review on Polymeric, Inorganic, and Composite Materials for Air Filters: From Processing to Properties. Advanced Energy and Sustainability Research, 2021, 2, 2100005.	5.8	20
66	Grafting and stabilization of ordered mesoporous silica COK-12 with graphene oxide for enhanced removal of methylene blue. RSC Advances, 2019, 9, 36271-36284.	3.6	19
67	Polymer derived ceramic aerogels. Current Opinion in Solid State and Materials Science, 2021, 25, 100936.	11.5	19
68	Crystallographic and electronic evolution of lanthanum strontium ferrite (La _{0.6} Sr _{0.4} FeO _{3â~î^}) thin film and bulk model systems during iron exsolution. Physical Chemistry Chemical Physics, 2019, 21, 3781-3794.	2.8	18
69	High specific surface area ordered mesoporous silica COK-12 with tailored pore size. Microporous and Mesoporous Materials, 2019, 280, 133-143.	4.4	18
70	In-vitro investigation of graphene oxide reinforced bioactive glass ceramics composites. Journal of Non-Crystalline Solids, 2019, 505, 122-130.	3.1	18
71	Review of space resources processing for Mars missions: Martian simulants, regolith bonding concepts and additive manufacturing. Open Ceramics, 2022, 9, 100216.	2.0	18
72	Surface modification of rice-husk ash (RHA) by Si3N4 coating to promote its wetting by Al-Mg-Si alloys. Materials Chemistry and Physics, 2018, 203, 223-234.	4.0	17

#	Article	IF	CITATIONS
73	Batch and continuous synthesis upscaling of powder and monolithic ordered mesoporous silica COK-12. Microporous and Mesoporous Materials, 2018, 256, 102-110.	4.4	17
74	In situ high pressure high temperature experiments in multi-anvil assemblies with bixbyite-type In2 O3 and synthesis of corundum-type and orthorhombic In2 O3 polymorphs. High Pressure Research, 2013, 33, 697-711.	1.2	16
75	Mechanistic in situ insights into the formation, structural and catalytic aspects of the La2NiO4 intermediate phase in the dry reforming of methane over Ni-based perovskite catalysts. Applied Catalysis A: General, 2021, 612, 117984.	4.3	16
76	Low temperature synthesis of nanocrystalline MnIn2O4 spinel. Dalton Transactions, 2012, 41, 3374.	3.3	15
77	Enhanced n-type thermopower in distortion-free LiMn2O4. Journal of Materials Chemistry, 2012, 22, 4631.	6.7	15
78	Hydrate Networks under Mechanical Stress - A Case Study for Co3(PO4)2·8H2O. European Journal of Inorganic Chemistry, 2016, 2016, 2072-2081.	2.0	15
79	Fabrication of cellular and lamellar LiFePO ₄ /C Cathodes for Li-ion batteries by unidirectional freeze-casting method. Journal of the Ceramic Society of Japan, 2016, 124, 1067-1071.	1.1	15
80	Ferroelectric InMnO3: Growth of single crystals, structure and high-temperature phase transitions. Journal of Solid State Chemistry, 2016, 241, 54-63.	2.9	15
81	Ferrimagnetism in manganese-rich gallium and aluminium spinels due to mixed valence Mn ²⁺ –Mn ³⁺ states. Dalton Transactions, 2018, 47, 2727-2738.	3.3	15
82	Metal-containing ceramic nanocomposites synthesized from metal acetates and polysilazane. Open Ceramics, 2020, 1, 100001.	2.0	15
83	Cu-Modified SrTiO ₃ Perovskites Toward Enhanced Water–Gas Shift Catalysis: A Combined Experimental and Computational Study. ACS Applied Energy Materials, 2021, 4, 452-461.	5.1	15
84	Mechanism of Gas Separation through Amorphous Silicon Oxycarbide Membranes. Advanced Engineering Materials, 2016, 18, 721-727.	3.5	14
85	Silicon oxycarbonitrides synthesized by ammonia-assisted thermolysis route from polymers: A total X-ray scattering, solid-state NMR, and TEM structural study. Journal of the European Ceramic Society, 2016, 36, 979-989.	5.7	14
86	Engaging the flux-grown La1â^'Sr Fe1â^'Ti O3 crystals in visible-light-driven photocatalytic hydrogen generation. International Journal of Hydrogen Energy, 2017, 42, 27024-27033.	7.1	14
87	Carbide-Modified Pd on ZrO2 as Active Phase for CO2-Reforming of Methane—A Model Phase Boundary Approach. Catalysts, 2020, 10, 1000.	3.5	14
88	Bispropylurea bridged polysilsesquioxane: A microporous MOF-like material for molecular recognition. Chemosphere, 2021, 276, 130181.	8.2	14
89	Atomic-Scale Insights into Nickel Exsolution on LaNiO ₃ Catalysts via <i>In Situ</i> Electron Microscopy. Journal of Physical Chemistry C, 2022, 126, 786-796.	3.1	14
90	Compressibility and structural stability of spinel-type MnIn2O4. Journal of Solid State Chemistry, 2015, 230, 301-308.	2.9	13

#	Article	IF	CITATIONS
91	Response of Gallium Nitride Chemiresistors to Carbon Monoxide is Due to Oxygen Contamination. ACS Sensors, 2017, 2, 713-717.	7.8	13
92	Surface chemistry and stability of metastable corundum-type In ₂ O ₃ . Physical Chemistry Chemical Physics, 2017, 19, 19407-19419.	2.8	13
93	Active Metal Electrode–Oxide Interface in Gas Sensor Operation Probed by In Situ and Timeâ€Resolved Xâ€Ray Spectroscopy. ChemPhysChem, 2010, 11, 79-82.	2.1	12
94	Indium hydroxide to oxide decomposition observed in one nanocrystal during in situ transmission electron microscopy studies. Journal of Solid State Chemistry, 2013, 198, 364-370.	2.9	12
95	H2 reduction of Gd- and Sm-doped ceria compared to pure CeO2 at high temperatures: effect on structure, oxygen nonstoichiometry, hydrogen solubility and hydroxyl chemistry. Physical Chemistry Chemical Physics, 2018, 20, 22099-22113.	2.8	12
96	Low-temperature fluoride-assisted synthesis of mullite whiskers. RSC Advances, 2020, 10, 31180-31186.	3.6	12
97	Stable anodes for lithium-ion batteries based on tin-containing silicon oxycarbonitride ceramic nanocomposites. Materials Today Energy, 2022, 26, 100989.	4.7	12
98	Ultramicroporous silicon nitride ceramics for CO ₂ capture. Journal of Materials Research, 2015, 30, 2958-2966.	2.6	11
99	Metastable Corundum-Type In ₂ O ₃ : Phase Stability, Reduction Properties, and Catalytic Characterization. Journal of Physical Chemistry C, 2016, 120, 15272-15281.	3.1	11
100	Hydrogen reduction and metal-support interaction in a metastable metal-oxide system: Pd on rhombohedral In2O3. Journal of Solid State Chemistry, 2018, 266, 93-99.	2.9	11
101	High-temperature structure of <mmi:math xmlns:mml="http://www.w3.org/1998/Math/MathML"><mml:mrow> <mml:msub> <mml:mi>Co</mml:mi> <mml: mathvariant="normal">O <mml:mn>4</mml:mn> </mml: </mml:msub> </mml:mrow> : Understanding spinel inversion using <i>in situ</i></mmi:math 	mn>33.2	nl:mn>11
102	B, 2019, 99, . Manufacturing and Characterization of Highly Porous Bioactive Glass Composite Scaffolds Using Unidirectional Freeze Casting. Advanced Engineering Materials, 2017, 19, 1700129.	3.5	10
103	Evaluating porous polylactide-co-glycolide/bioactive glass composite microsphere powders for laser sintering of scaffolds. Powder Technology, 2019, 354, 289-300.	4.2	10
104	Fabrication of polymer-derived ceramics with hierarchical porosities by freeze casting assisted by thiol-ene click chemistry and HF etching. Journal of the European Ceramic Society, 2020, 40, 315-323.	5.7	10
105	Springback effect and structural features during the drying of silica aerogels tracked by in-situ synchrotron X-ray scattering. Scientific Reports, 2022, 12, 7537.	3.3	10
106	Pressure-Induced Decomposition of Indium Hydroxide. Journal of the American Chemical Society, 2010, 132, 12674-12678.	13.7	9
107	Kinetic control in the synthesis of metastable polymorphs: Bixbyite-to-Rh2O3(II)-to-corundum transition in In2O3. Journal of Solid State Chemistry, 2015, 229, 278-286.	2.9	9
108	Scaled-up solvothermal synthesis of nanosized metastable indium oxyhydroxide (InOOH) and corundum-type rhombohedral indium oxide (rh-In ₂ O ₃). Zeitschrift Fur Kristallographie - Crystalline Materials, 2017, 232, 129-140.	0.8	9

#	Article	IF	CITATIONS
109	Fabrication and Characterization of Ice Templated Membrane Supports from Portland Cement. Membranes, 2020, 10, 93.	3.0	9
110	Effect of <i>Fomes fomentarius</i> Cultivation Conditions on Its Adsorption Performance for Anionic and Cationic Dyes. ACS Omega, 2022, 7, 4158-4169.	3.5	9
111	Solar hydrogen generation using niobium-based photocatalysts: design strategies, progress, and challenges. Materials Today Energy, 2022, 24, 100936.	4.7	9
112	Ceramic Stereolithography of Bioactive Glasses: Influence of Resin Composition on Curing Behavior and Green Body Properties. Biomedicines, 2022, 10, 395.	3.2	9
113	Fabrication and characterization of porous mullite ceramics derived from fluoride-assisted Metakaolin-Al(OH)3 annealing for filtration applications. Open Ceramics, 2022, 9, 100240.	2.0	9
114	Extrusion-based additive manufacturing of fungal-based composite materials using the tinder fungus Fomes fomentarius. Fungal Biology and Biotechnology, 2021, 8, 21.	5.1	9
115	Synthesemethoden für keramische Materialien. Hochtechnologiewerkstoffe. Chemie in Unserer Zeit, 2010, 44, 208-227.	0.1	8
116	Electrochemical study of NiO nanosheets: toward the understanding of capacity fading. Journal of Materials Science, 2017, 52, 6498-6505.	3.7	8
117	Delayed release of chemokine CCL25 with bioresorbable microparticles for mobilization of human mesenchymal stem cells. Acta Biomaterialia, 2018, 69, 290-300.	8.3	8
118	Revised model for thermopower and site inversion in <mml:math xmlns:mml="http://www.w3.org/1998/Math/MathML"><mml:mrow><mml:msub><mml:mi>Co</mml:mi><mml: mathvariant="normal">O<mml:mn>4</mml:mn></mml: </mml:msub></mml:mrow> spinel. Physical Review B, 2018, 98, .</mml:math 	mnչ3 <td>nl:mn></td>	nl:mn>
119	Ceria-Based Dual-Phase Membranes for High-Temperature Carbon Dioxide Separation: Effect of Iron Doping and Pore Generation with MgO Template. Membranes, 2019, 9, 108.	3.0	8
120	Silicon oxycarbonitride ceramic containing nickel nanoparticles: from design to catalytic application. Materials Advances, 2021, 2, 1715-1730.	5.4	8
121	Zirconium Oxycarbide: A Highly Stable Catalyst Material for Electrochemical Energy Conversion. ChemPhysChem, 2019, 20, 3067-3073.	2.1	6
122	AlF3-assisted flux growth of mullite whiskers and their application in fabrication of porous mullite-alumina monoliths. Open Ceramics, 2021, 7, 100145.	2.0	6
123	Elucidating the role of earth alkaline doping in perovskite-based methane dry reforming catalysts. Catalysis Science and Technology, 2022, 12, 1229-1244.	4.1	6
124	Insights into the Mechanism of Gas Sensor Operation. , 2013, , 3-34.		5
125	Perovskiteâ€type Solid Solution SrMo _{1–<i>x</i>} W <i>_x</i> (O, N) ₃ Oxynitrides: Synthesis, Structure, and Magnetic Properties. Zeitschrift Fur Anorganische Und Allgemeine Chemie, 2015, 641, 1533-1539.	1.2	5
126	Iron Exsolution Phenomena in Lanthanum Strontium Ferrite SOFC Anodes. ECS Transactions, 2017, 78, 1327-1341.	0.5	5

Aleksander Gurlo

#	Article	IF	CITATIONS
127	<i>trans</i> -Bis(acetato-îº <i>O</i>)bis(2-aminoethanol-îº ² <i>N</i> , <i>O</i>)nickel(II). Acta Crystallographica Section E: Structure Reports Online, 2012, 68, m567-m568.	0.2	4
128	Phase segregation in Mn-doped In2O3: in situ high-pressure high-temperature synchrotron studies in multi-anvil assemblies. RSC Advances, 2013, 3, 5357.	3.6	4
129	Inkjetâ€Printed Nanoscaled CuO for Miniaturized Gasâ€5ensing Devices. European Journal of Inorganic Chemistry, 2013, 2013, 1481-1487.	2.0	4
130	Influence of Composition on Mechanical Properties of Additively Manufactured Composites Reinforced with Endless Carbon Fibers. Key Engineering Materials, 2019, 809, 335-340.	0.4	4
131	Treading in the Limited Stability Regime of Lanthanum Strontium Ferrite — Reduction, Phase Change and Exsolution. ECS Transactions, 2019, 91, 1771-1781.	0.5	4
132	Real-time direct transmission electron microscopy imaging of phase and morphology transformation from solid indium oxide hydroxide to hollow corundum-type indium oxide nanocrystallites. Nanoscale, 2019, 11, 12242-12249.	5.6	4
133	Synthesis and rapid sintering of dense SrA(O,N)3 (A=Mo, W) oxynitride ceramics. Journal of the European Ceramic Society, 2015, 35, 3273-3281.	5.7	3
134	Formation of Pd-Ce intermetallic compounds by reductive metal-support interaction. Journal of Solid State Chemistry, 2018, 265, 176-183.	2.9	3
135	Steering the methanol steam reforming reactivity of intermetallic Cu–In compounds by redox activation: stability <i>vs.</i> formation of an intermetallic compound–oxide interface. Catalysis Science and Technology, 2021, 11, 5518-5533.	4.1	3
136	CrabNet for Explainable Deep Learning in Materials Science: Bridging the Gap Between Academia and Industry. Integrating Materials and Manufacturing Innovation, 2022, 11, 41-56.	2.6	3
137	A comparison of syntheses approaches towards functional polycrystalline silicate ceramics. Open Ceramics, 2022, 9, 100241.	2.0	3
138	Orthorhombisches In ₂ O ₃ – ein metastabiles Indiumsesquioxid―Polymorph. Angewandte Chemie, 2013, 125, 6659-6663.	2.0	2
139	Shape-, size- and phase-controlled indium oxide for gas sensing. , 2008, , .		1
			_

140 Sensing in harsh conditions: How to protect SnO<inf>2</inf> sensing layer. , 2010, , .